Wave reflection at the interface between a nonlinear discrete lattice and a matching linear system

Hoving, Jeroen; Metrikine, Andrei

Publication date
2017

Document Version
Final published version

Published in
ICSV24 – International Congress on Sound and Vibration, July 23-27, 2017, London, UK

24th INTERNATIONAL CONGRESS ON SOUND AND VIBRATION
23–27 July 2017, London

ICSV24
23-27JULY 2017
LONDON CALLING

WAVE REFLECTION AT THE INTERFACE BETWEEN A NONLINEAR DISCRETE LATTICE AND A MATCHING LINEAR SYSTEM

Jeroen Hoving and Andrei Metrikine

Delft University of Technology, Faculty of Civil Engineering and Geosciences, Delft, the Netherlands
email: j.s.hoving@tudelft.nl

This contribution considers the wave reflection at the interface between a discrete lattice that describes the nonlinear near-field response to a dynamic load and a matching system that describes the linear far-field response. The near-field system is modelled as a one-dimensional discrete system of particles that is capable of describing nonlinear behaviour by including dry friction. The purpose of coupling this nonlinear near-field system to a linear far-field system is to optimize for computational efficiency as, in the time domain, the linear far-field system can be replaced by a single integral force-displacement relation. In the frequency domain, this relation is commonly known as the dynamic stiffness, or inversely, as the dynamic compliance. For an ideal coupling between the two systems an incident wave should propagate through the interface undisturbed and without reflections. For long incident waves, it would suffice to describe the far-field system by a classical continuum, however for short incident waves, the reflections of the classical continuum are significant. Therefore, the linear far-field system is described as a semi-infinite discrete particle system, also known as a semi-infinite cascade, that matches the discrete nature of the near-field lattice. To assess the quality of the applied coupling, we consider the reflection of an incident wave at the lattice-cascade interface, using both time and frequency domain approaches, and compare it to the reflection at the interface of a system where the far-field system is described by a semi-infinite continuum.

Keywords: wave reflection, non-smooth dynamics, multi-scale, hybrid modelling.

1. Introduction

As nonlinear phenomena are difficult to capture by continuum models, many applications are found where the response of a medium is modelled using discrete approaches [1-4]. These models require a nonlinear analysis of the material behaviour, but only at certain segments where deformations are significant and failure may occur, e.g. near a load source or at the interface between two bodies. For the remainder of the medium linear modelling is generally sufficient. For numerical analysis, it is profitable to describe such a medium using a hybrid model that consists of a sophisticated discrete segment, able to account for nonlinear phenomena, and of a linear segment, which, in the time domain, can be replaced by an integral force-displacement relation. In the frequency domain, this relation is commonly known as the dynamic stiffness.

In this contribution, we consider a one-dimensional semi-infinite medium that consists of a discrete lattice that describes the nonlinear near-field response to a dynamic load, and a matching linear system that describes the far-field response. For long incident waves, the far-field system may be well described by a continuum. For short incident waves however, the reflections of the continuum may be significant as its dispersive properties are different from those of the near-field lattice. For the far-field therefore, a discrete particle system, also known as a cascade [5], is introduced that matches the discrete nature of the near-field lattice. Fig. 1 shows the near-field lattice respectively coupled to a) a semi-infinite viscoelastic rod, and b) a semi-infinite viscoelastic cascade. The near-field lattice is connected to either far-field system at the semi-particle **N** with coordinate x_{Int}. The

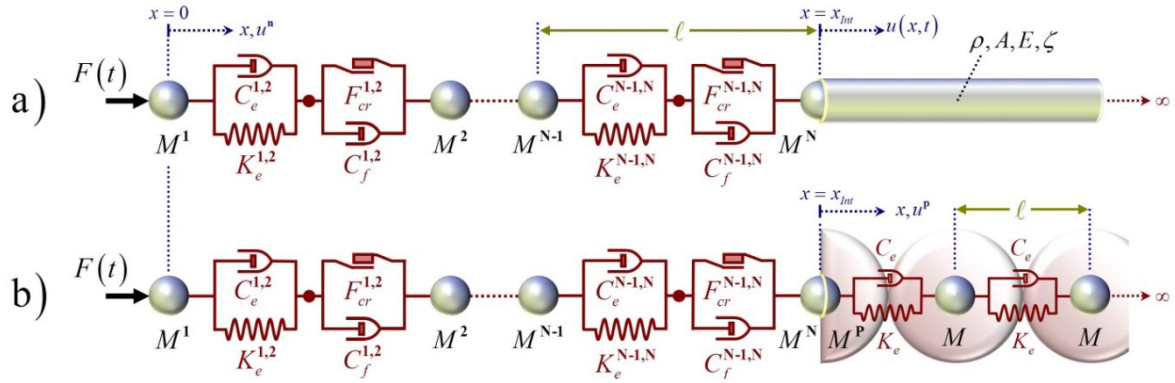

Fig. 1: The one-dimensional Bingham-Kelvin-Voigt lattice coupled to:
a) a semi-infinite viscoelastic rod; b) a semi-infinite viscoelastic cascade.

location of the interface is chosen at such distance from an applied time-dependent load that nonlinear phenomena occur exclusively in the lattice, while the lattice behaves linearly near the interface.

2. Properties and governing equations of the near-field lattice

As depicted in Fig. 1, the near-field lattice consists of **N** particles, where every particle **n** has a mass $M^{\mathbf{n}}$ and the unit distance between particles is equal to ℓ. The elements in the near-field lattice are composed of a viscoelastic Kelvin-Voigt element and a viscoplastic Bingham element in series. These elements are referred to as Bingham-Kelvin-Voigt elements or, in short, BKV elements. Any Kelvin-Voigt element between particles **n** and **n+1** has a stiffness $K_e^{\mathbf{n},\mathbf{n+1}}$ and a damping $C_e^{\mathbf{n},\mathbf{n+1}}$, while the corresponding Bingham element has a damping $C_f^{\mathbf{n},\mathbf{n+1}}$. Additionally, the Bingham element is only activated once the force on the Bingham element becomes larger than the threshold of the dry friction element, i.e. the critical friction force $F_{cr}^{\mathbf{n},\mathbf{n+1}}$. Each BKV element behaves according to different motion states; the motion state where the Bingham element is not activated is referred to as "stick", while the motion state for which the Bingham element is activated is referred to as "slip". The system of equations of motion for the particles $\mathbf{n}=\mathbf{1}...\mathbf{N-1}$ in the BKV lattice reads:

$$M^{\mathbf{1}}\ddot{u}^{\mathbf{1}} - C_e^{\mathbf{1,2}}\dot{e}_{\text{state}}^{\mathbf{1,2}} - K_e^{\mathbf{1,2}}e_{\text{state}}^{\mathbf{1,2}} = F(t) \tag{1}$$

$$M^{\mathbf{n}}\ddot{u}^{\mathbf{n}} + F_{\text{state}}^{\mathbf{n-1,n}} - C_e^{\mathbf{n,n+1}}\dot{e}_{\text{state}}^{\mathbf{n,n+1}} - K_e^{\mathbf{n,n+1}}e_{\text{state}}^{\mathbf{n,n+1}} = 0 \tag{2}$$

Here, $u^{\mathbf{n}}$ is the longitudinal displacement of particle **n**, $F(t)$ is a time-dependent force applied at particle **1** and Newton's or dot notation is used for differentiation to time. Furthermore, depending on the involved motion state, $e_{\text{state}}^{\mathbf{n},\mathbf{n+1}}$ gives the relevant elongation of the element between particles **n** and **n+1**, while $F_{\text{state}}^{\mathbf{n-1,n}}$ describes the force that is applied by the BKV element between particles **n-1** and **n** to the particle **n**. The corresponding expressions for respectively stick and slip are:

$$\begin{cases} e_{\text{stick}}^{\mathbf{n},\mathbf{n+1}} = e^{\mathbf{n},\mathbf{n+1}} - \varepsilon_B^{\mathbf{n},\mathbf{n+1}} \\ e_{\text{slip}}^{\mathbf{n},\mathbf{n+1}} = e_{KV}^{\mathbf{n},\mathbf{n+1}} \end{cases}, \qquad \begin{cases} F_{\text{stick}}^{\mathbf{n-1,n}} = C_e^{\mathbf{n-1,n}}\dot{e}^{\mathbf{n-1,n}} + K_e^{\mathbf{n-1,n}}\left(e^{\mathbf{n-1,n}} - \varepsilon_B^{\mathbf{n-1,n}}\right) \\ F_{\text{slip}}^{\mathbf{n-1,n}} = C_f^{\mathbf{n-1,n}}\dot{e}_B^{\mathbf{n-1,n}} + F_{cr}^{\mathbf{n-1,n}}\,\text{sgn}\,F_{B:\text{slip}}^{\mathbf{n-1,n}} \end{cases}. \tag{3}$$

For a BKV element in slip, the equation of motion for the node in-between the Kelvin-Voigt and Bingham elements, must be included; for the node between particles **n** and **n+1** this equation reads:

$$C_e^{\mathbf{n},\mathbf{n+1}}\dot{e}_{KV}^{\mathbf{n},\mathbf{n+1}} + K_e^{\mathbf{n},\mathbf{n+1}}e_{KV}^{\mathbf{n},\mathbf{n+1}} - C_f^{\mathbf{n},\mathbf{n+1}}\dot{e}_B^{\mathbf{n},\mathbf{n+1}} - F_{cr}^{\mathbf{n},\mathbf{n+1}}\,\text{sgn}\,F_{B:\text{slip}}^{\mathbf{n},\mathbf{n+1}} = 0 \tag{4}$$

Here, $e^{\mathbf{n},\mathbf{n+1}}$, $e_{KV}^{\mathbf{n},\mathbf{n+1}}$ and $e_B^{\mathbf{n-1,n}}$ respectively describe the elongation of the BKV, the Kelvin-Voigt- and the Bingham elements between adjacent particles, while $\varepsilon_B^{\mathbf{n},\mathbf{n+1}}$ denotes the constant elongation of the Bingham element when it is inactive. Then, $F_{B:\text{slip}}^{\mathbf{n},\mathbf{n+1}}$ denotes the force on the Bingham element, so that $\text{sgn}\,F_{B:\text{slip}}^{\mathbf{n},\mathbf{n+1}}$ determines the sign of the critical friction force $F_{cr}^{\mathbf{n},\mathbf{n+1}}$ based on whether the current instance of slip was initiated in tension of in compression. Note here that the sign of the critical friction force remains the same throughout each instance of slip [6].

3. Coupling the near-field lattice to a matching linear far-field system

To correctly describe the behaviour of an environment composed of two systems, any incident waves should ideally propagate through their interface undisturbed and without reflections. Moreover, when the far-field system is semi-infinite, the interface should ideally be silent and the far-field system should provide the near-field lattice with a non-reflective boundary. To assure this, the BKV lattice and the far-field system must at least have matching material properties in the region of the interface. For the semi-infinite cascade, we conveniently also match the discrete properties, so that, in the region of the interface, the unit distance ℓ and thereby the particle mass M, as well as the damping C_e and the stiffness K_e are the same in both systems.

The relation between the material properties of the cascade and the rod is established by matching the equation of motion for the cascade in the long-wave limit, by applying the Taylor expansion [7], with the equation of motion for the rod. Denoting density, cross-section area, Young's modulus and damping coefficient of the rod as ρ, E, A and ζ respectively, and noting that the mass per unit length of cascade and rod must coincide, we find the relations between their material properties as:

$$M = \rho A \ell, \quad C_e = \zeta K_e, \quad K_e = \frac{EA}{\ell}. \tag{5}$$

Note here that the viscous damping in the rod is included through the dynamic modulus of elasticity $\hat{E}$, which describes the viscoelastic behaviour of the rod as $\hat{E} = E\left(1+\zeta \frac{\partial}{\partial t}\right)$.

To apply the coupling of the BKV lattice with either far-field system, we consider their interaction as a boundary value problem for the far-field system, consisting of the equation of motion for the far-field system, as well as the force equilibrium and the displacement relation at their interface.

3.1 Dynamic stiffness of the semi-infinite viscoelastic rod

To compare the considered far-field systems, we normalize the coupled lattice-rod system by introducing the following dimensionless parameters for time, space and material properties:

$$t = t_{\mathrm{dim}}\omega_0, \quad x = \frac{x_{\mathrm{dim}}}{\ell}, \quad \zeta = \frac{\zeta_{\mathrm{dim}} c}{2\ell}, \quad M^{\mathbf{n}} = \frac{M^{\mathbf{n}}_{\mathrm{dim}}}{\rho A \ell}, \quad C_e^{\mathbf{n,n+1}} = \frac{C^{\mathbf{n,n+1}}_{e;\mathrm{dim}}}{\rho A c}, \quad K_e^{\mathbf{n,n+1}} = \frac{K^{\mathbf{n,n+1}}_{e;\mathrm{dim}}\ell}{EA}. \tag{6}$$

Here, ω_0 is the natural frequency of the homogeneous BKV lattice, c is the longitudinal wave velocity in the rod, ζ is the damping ratio and the subscript dim is used for dimensional variables.

For the interaction of the BKV lattice with the viscoelastic rod, the force equilibrium follows from the equation of motion of the semi-particle **N**, the stress in the rod and Hooke's Law that incorporates the damping through the dynamic modulus of elasticity. Additionally, the displacement of the semi-particle **N** must be equal to the displacement of the tip of the rod. Applying the Laplace integral transform with respect to time, the dimensionless coupling statement reads:

$$s^2\tilde{u}(x,s) - (2\zeta s+1)\tilde{u}''(x,s) = 0 \tag{7}$$

$$(2\zeta s+1)\tilde{u}'(x_{Int},s) = M^{\mathbf{N}}s^2\tilde{u}^{\mathbf{N}} + \left(C_e^{\mathbf{N\text{-}1,N}}s + K_e^{\mathbf{N\text{-}1,N}}\right)\tilde{e}^{\mathbf{N\text{-}1,N}} \tag{8}$$

$$\tilde{u}(x_{Int},s) = \tilde{u}^{\mathbf{N}} \tag{9}$$

Here, the tilde over a variable denotes that variable as its Laplace transform and s is the dimensionless complex-valued Laplace parameter. Accounting for the appropriate behaviour of the viscoelastic rod at infinity and substituting the general solution to Eq. (7), as well as Eq. (9), into Eq. (8), yields the equation of motion for the semi-particle **N** in the Laplace domain as:

$$M^{\mathbf{N}}s^2\tilde{u}^{\mathbf{N}} + \left(C_e^{\mathbf{N\text{-}1,N}}s + K_e^{\mathbf{N\text{-}1,N}}\right)\tilde{e}^{\mathbf{N\text{-}1,N}} + \chi(s)\tilde{u}^{\mathbf{N}} = 0 \tag{10}$$

Here, the dynamic stiffness $\chi(s)$ of the viscoelastic rod is found as:

$$\chi(s) = s\sqrt{2\zeta s+1} \tag{11}$$

3.2 Dynamic stiffness of the semi-infinite viscoelastic cascade

To normalize the coupled lattice-cascade system, we introduce the following dimensionless parameters for time, space and material properties:

$$t = t_{\mathrm{dim}}\omega_0, \quad x = \frac{x_{\mathrm{dim}}}{\ell}, \quad M^{\mathbf{n}} = \frac{M^{\mathbf{n}}_{\mathrm{dim}}}{M}, \quad C_e^{\mathbf{n,n+1}} = \frac{C^{\mathbf{n,n+1}}_{e;\mathrm{dim}}}{M\omega_0}, \quad K_e^{\mathbf{n,n+1}} = \frac{K^{\mathbf{n,n+1}}_{e;\mathrm{dim}}}{K_e}. \tag{12}$$

Here, ω_0 is the natural frequency of both the homogeneous BKV lattice and the cascade, and as before, the subscript dim is used to denote dimensional variables. Describing the dimensionless properties of the cascade accordingly, the dimensionless mass, damping and stiffness inside the cascade are respectively found as $M = 1$, $C_e = 2\zeta$ and $K_e = 1$, where ζ denotes the damping ratio.

To distinguish the particles in the cascade from those of the BKV lattice, these particles are referred to using numerator **p** and the semi-particle at the tip of the cascade is referred to as particle **P**. The force equilibrium at the interface between the BKV lattice and the cascade then follows from the equations of motion of the semi-particles **N** and **P**, while the displacement constraint states that the displacements of the two semi-particles must be the same. Applying the Laplace integral transform with respect to time, the dimensionless coupling statement thus becomes:

$$s^2\tilde{u}^{\mathbf{p}}(s) + (2\zeta s + 1)\left(2\tilde{u}^{\mathbf{p}}(s) - \tilde{u}^{\mathbf{p-1}}(s) - \tilde{u}^{\mathbf{p+1}}(s)\right) = 0 \tag{13}$$

$$-M^{\mathbf{P}}s^2\tilde{u}^{\mathbf{P}}(s) - (2\zeta s + 1)\left(\tilde{u}^{\mathbf{P}}(s) - \tilde{u}^{\mathbf{P+1}}(s)\right) = M^{\mathbf{N}}s^2\tilde{u}^{\mathbf{N}} + \left(C_e^{\mathbf{N-1,N}}s + K_e^{\mathbf{N-1,N}}\right)\tilde{e}^{\mathbf{N-1,N}} \tag{14}$$

$$\tilde{u}^{\mathbf{P}}(s) = \tilde{u}^{\mathbf{N}} \tag{15}$$

Here, $M^{\mathbf{P}}$ denotes the mass of the semi-particle **P** at the tip of the cascade. As the tilde is used to denote a variable as its Laplace transform, $\tilde{u}^{\mathbf{p}}(s)$ denotes the longitudinal displacement of a particle **p** in the cascade that, accounting for the appropriate behaviour of the cascade at infinity, is assumed as $\tilde{u}^{\mathbf{p}}(s) = Ae^{-\mathrm{i}\kappa\mathbf{p}}$. Substituting this assumed displacement into Eq. (15) yields the Laplace domain displacement of particle **p** as $\tilde{u}^{\mathbf{p}}(s) = \tilde{u}^{\mathbf{N}}e^{-\mathrm{i}\kappa(\mathbf{p}-\mathbf{P})}$. Then, substituting the resulting expression into Eq. (14), the equation of motion for the semi-particle **N** is found to coincide with Eq. (10), except that the expression for the dynamic stiffness of the cascade reads:

$$\chi(s) = M^{\mathbf{P}}s^2 + (2\zeta s + 1)\left(1 - e^{-\mathrm{i}\kappa}\right) \tag{16}$$

The dynamic stiffness of the semi-infinite viscoelastic cascade is here given in terms of both the Laplace parameter s and the dimensionless wavenumber κ. The dispersion relation for the viscoelastic cascade may be obtained from the homogeneous equation of motion of the cascade and reads:

$$s^2 + (2\zeta s + 1)4\sin^2\frac{\kappa}{2} = 0 \tag{17}$$

From the dispersion relation, we can derive the following useful relations between the dimensionless wavenumber κ and the dimensionless Laplace parameter s:

$$\cos\kappa = 1 + \frac{\frac{1}{2}s^2}{2\zeta s + 1}, \quad \sin\kappa = \frac{-\mathrm{i}s}{2\zeta s + 1}\sqrt{2\zeta s + 1 + \tfrac{1}{4}s^2}\,. \tag{18}$$

Note here that, to obtain the correct sine relation from the given cosine relation, the branch of the square root must be chosen such that the imaginary part of the wavenumber κ is negative and thereby corresponds to the forward propagating wave that fades for $\mathbf{p} \to \infty$.

Rearranging Eq. (16) using Euler's formula and substituting the relations from Eq. (18), the dynamic stiffness of the viscoelastic cascade, exclusively in terms of the Laplace parameter s, reads:

$$\chi(s) = M^{\mathbf{P}}s^2 - \tfrac{1}{2}s^2 + s\sqrt{2\zeta s + 1 + \tfrac{1}{4}s^2} \tag{19}$$

In the form of Eq. (19), the dynamic stiffness of the viscoelastic cascade depends on the dimen-

sionless mass $M^{\mathbf{P}}$ of the semi-particle **P**. The influence of varying the mass $M^{\mathbf{P}}$ on the response of a cascade has previously been investigated in [5]. By substituting Eq. (19) into Eq. (10) however, it can be straightforwardly derived that the inertial term in the remaining interface equation is related to the combined mass of the semi-particles **N** and **P**, which due to homogeneity must be equal to the mass M, i.e. $M^{\mathbf{N}} + M^{\mathbf{P}} = M$. Thus, by choosing the interface between the near- and far-field systems at a particle, it follows that the semi-particles **N** and **P** both represent half the particle spacing, so that $M^{\mathbf{N}} = M^{\mathbf{P}} = \frac{1}{2}$. Note here that, depending on the chosen point of coupling, different combinations of the interface mass and stiffness exist at which there will be no reflection at the interface between the near- and the far-field systems [8]. Nevertheless, for the current geometry, the dynamic stiffness of the semi-infinite viscoelastic cascade may be obtained from Eq. (19) as:

$$\chi(s) = s\sqrt{2\zeta s + 1 + \tfrac{1}{4}s^2} \tag{20}$$

3.3 Comparison of the dynamic stiffnesses for the cascade and the rod

Comparing the expressions for the dynamic stiffness of the semi-infinite viscoelastic cascade with that of the rod, respectively given by Eqs. (20) and (11), the Laplace domain expression for the dynamic stiffness of the cascade additionally includes a term $\frac{1}{4}s^2$ under the square root. This implies that the difference between the dynamic stiffnesses of cascade and rod will be small for $s<1$, i.e. for low frequencies, while the difference may be significant for $s>1$, i.e. for frequencies higher than the natural frequency. This is testified by Fig. 2a in which the continuous green line gives the absolute value of the dynamic stiffness of the semi-infinite viscoelastic cascade as a function of dimensionless frequency, while the continuous red and blue lines give the absolute values of the corresponding real and imaginary parts respectively. Additionally, the dashed green, blue and red lines give the absolute values of the dynamic stiffness of the semi-infinite viscoelastic rod, as well as the absolute values of its real and imaginary parts respectively. The difference between the dynamic stiffnesses of cascade and rod appears to be negligible for frequencies that are much lower than the natural frequency, i.e. for long waves. The differences between cascade and rod however are apparent when higher frequencies, i.e. short waves, are considered. This supports the notion that for long incident waves, it would suffice to describe the far-field system by a classical continuum, while for shorter incident waves, the reflections from the classical continuum may be significant.

3.4 Interface equation in the time domain

For the far-field systems considered here, it is not possible to obtain time-domain expressions for the dynamic stiffnesses analytically and therefore they must be obtained numerically [6]. Numerically applying the inverse Laplace transform requires the truncation of its infinite domain of integration, which is only allowed if the integrand is sufficiently convergent. As shown by Fig. 2a, the dynamic stiffnesses of both far-field systems are not convergent at all. To overcome this, we con-

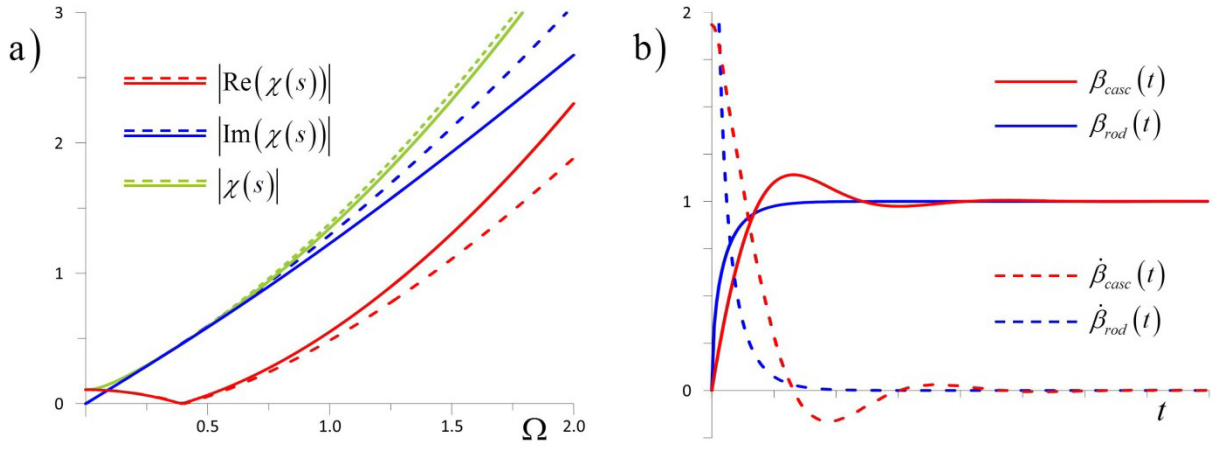

Fig. 2: a) Dynamic stiffnesses of the semi-infinite viscoelastic cascade (solid) and the semi-infinite viscoelastic rod (dashed) in the frequency domain; b) Dynamic compliances and admittances in the time domain.

sider the interaction between the near-field lattice and the far-field systems using the dynamic compliance, i.e. the inverse of the dynamic stiffness, instead. Applying the inverse Laplace transforms to the dynamic compliances of the cascade and the rod, respectively given by the inverse of Eqs. (11) and (20), yields the dynamic compliances in the time domain respectively as:

$$\beta_{casc}(t) = 2\int_0^t e^{-4\zeta\tau} J_0\left(2\tau\sqrt{1-4\zeta^2}\right) d\tau, \qquad \beta_{rod}(t) = \operatorname{erf}\sqrt{\frac{t}{2\zeta}}. \tag{21}$$

Here, erf denotes the (Gauss) error function and $J_0(..)$ denotes the Bessel function of the first kind of order zero. The time domain dynamic compliances for the cascade and the rod are given by respectively the continuous red and blue lines in Fig. 2b.

The Laplace domain interface equation is obtained in terms of the dynamic compliance by dividing Eq. (10) by the dynamic stiffness, or alternatively by multiplying with the dynamic compliance. Then, applying the inverse Laplace transform and subsequently differentiating the resulting equation using Leibniz' rule for differentiation of integrals [9] to obtain the contribution of the convolution integral to the current integration step, as well as taking into account that for both systems $\beta(t=0)=0$, the equation of motion for the interface particle **N** in the time domain becomes:

$$\ddot{u}^{\mathbf{N}} + \int_0^t \dot{\beta}(t-\tau)\left\{M^{\mathbf{N}}\ddot{u}^{\mathbf{N}} + C_e^{\mathbf{N\text{-}1,N}}\dot{e}^{\mathbf{N\text{-}1,N}} + K_e^{\mathbf{N\text{-}1,N}}e^{\mathbf{N\text{-}1,N}}\right\}(\tau)\, d\tau = 0 \tag{22}$$

Here, $\dot{\beta}(t)$ is the time-derivative of the time-domain dynamic compliance, which can be considered as a time-domain expression for the admittance, as the corresponding Laplace-domain expression equals the inverse of the impedance. The time domain admittances for the semi-infinite viscoelastic cascade and the semi-infinite viscoelastic rod are depicted in Fig. 2b by respectively the dashed red and blue lines. The corresponding expressions are respectively found as:

$$\dot{\beta}_{casc}(t) = 2e^{-4\zeta t} J_0\left(2t\sqrt{1-4\zeta^2}\right), \qquad \dot{\beta}_{rod}(t) = \frac{e^{-\frac{1}{2}t/\zeta}}{\sqrt{2\pi\zeta t}}. \tag{23}$$

In the time domain, the system of equations of motion, consisting of Eqs. (1) - (4) and Eq. (22), is solved numerically using a Runge-Kutta method. Consequently, the contribution of Eq. (22) to the current integration step must be extracted from the convolution integral using a numerical integration scheme such as the composite trapezium rule. For the cascade, this is straightforward as the time-domain admittance of the cascade at $t=0$ is found as $\dot{\beta}(0)=2$. The time domain admittance of the rod however is infinite at $t=0$. Despite the singularity however, the contribution of the convolution integral to the current time step Δt, i.e. the integration over the domain $\tau = t-\Delta t \ldots t$, can be obtained analytically by assuming that within this time step the part of the convolution integral in Eq. (22) between accolades is a linear function. This is well within the error of applying the trapezium rule, for which the whole integrand is assumed to be linear between any two integration points.

4. Response of the coupled systems

Fig. 3 depicts the longitudinal response of the one-dimensional BKV system due to a single-sinus pulse load at ten consecutive time moments. Here, only the displacement response of the near-field BKV lattice, consisting of 80 particles, is shown. The amplitude and angular frequency of the pulse load are chosen as $\bar{F}=1\,\mathrm{MN}$ and $\omega=250\,\mathrm{rad/s}$. The properties of the rod are chosen as $\rho=2000\,\mathrm{kg/m^3}$, $A=1\,\mathrm{m^2}$, $E=20\,\mathrm{MPa}$ and $\zeta=0{,}1$. Additionally, choosing the unit interparticle distance as $\ell=0{,}2\,\mathrm{m}$, the dimensional properties of the cascade are $M=400\,\mathrm{kg}$, $K_e=100\,\mathrm{MN/m}$ and $C_e=C_f=40\,\mathrm{kNs/m}$. This yields a natural frequency $\omega_0=500\,\mathrm{rad/s}$, so that the dimensionless frequency of the single-sinus pulse is equal to $\Omega=0{,}5$.

As the material properties of all particles and elements in the BKV lattice are denoted separately using the numerator **n**, the material properties can be varied along the one-dimensional BKV lattice.

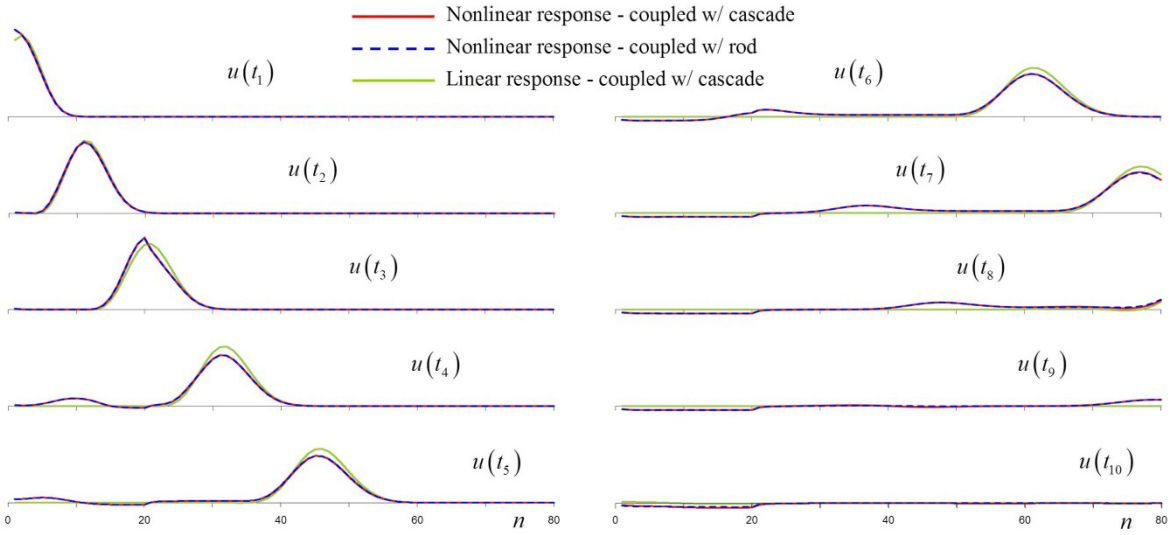

Fig. 3: Longitudinal displacement along the one-dimensional BKV-system at consecutive times.

To obtain the linear response, given in Fig. 3 by the continuous green line, the critical friction force of all elements was chosen as $F_{cr} > \overline{F}$ so that the dry friction elements were not activated, while all other properties were chosen to coincide with those of the cascade. The continuous red and dashed blue lines in Fig. 3 give the nonlinear response of BKV lattice coupled to respectively the cascade and the rod. For the nonlinear responses, the critical friction force of the BKV elements was generally chosen as $F_{cr} = 0,8\overline{F}$. Additionally, to amplify nonlinear effects, the critical friction force and damping ratio of the elements between particles $\mathbf{n} = 20\ldots40$ were reduced to $F_{cr}^{\mathbf{n,n+1}} = 0,4\overline{F}$ and $C_e^{\mathbf{n,n+1}} = C_f^{\mathbf{n,n+1}} = 32\,\mathrm{kNs/m}$ respectively.

Fig. 3 shows that for the nonlinear response, the incident wave is partially reflected at the edges of the weak segment of the lattice. This secondary wave first propagates towards the tip of the lattice and then reflects at the tip before it is eventually transmitted into the far-field domain. Due to occurring nonlinear events, the first segment of the BKV lattice remains displaced. Note that, at the scale of Fig. 3, the difference between the coupling with either cascade or rod is not distinguishable.

To assess the quality of the coupling between BKV lattice and respectively cascade and rod, we consider the reflection of an incident wave at their interface for a near-field-lattice that behaves exclusively linear. The resulting reflections are depicted in Fig. 4 at four consecutive time moments, where the upper graph shows the moment in time at which the incident wave has almost fully been transmitted into the far-field domain. While Fig. 4a shows the reflections obtained by solving the governing system of equations in the time domain using a Runge-Kutta method, Fig. 4b shows the reflections obtained by solving the system of equations algebraically in the Laplace domain and subsequently applying the inverse Laplace transform numerically at every time step. Note that while the scale of Fig. 4a and Fig. 4b is the same, their scale is 40 times smaller than the scale of Fig. 3.

5. Discussion and Conclusions

Comparing the reflections in Fig. 4a, it is striking that the reflection at the lattice-cascade interface is larger than the reflection at the lattice-rod interface. As the geometry of lattice and cascade is identical and they have the same dispersive properties, one would expect that the reflection at the lattice-cascade interface would be smaller than the reflection at the interface between lattice and rod, which are fundamentally different and have different dispersive properties. The latter is verified by the reflections obtained using the frequency-domain solution depicted in Fig. 4b, where the lattice-cascade interface is completely non-reflective and the lattice-rod interface shows a small reflection. From the comparison with Fig. 4b, it follows that the reflection in Fig. 4a must be due to numerical errors that are significantly larger at the lattice-cascade interface than at the lattice-rod interface. This can be explained by the method applied to solve the interface equation. For the lattice-cascade interface, the contribution of the convolution integral to the current time step is ob-

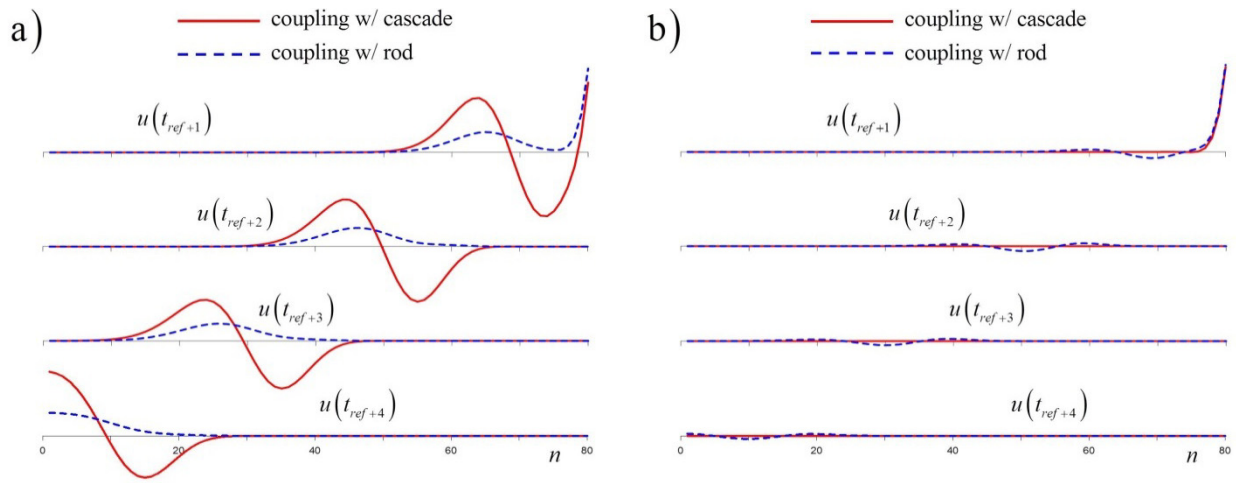

Fig. 4: Reflection of the longitudinal wave along the linearly behaving BKV-system:
a) time-domain solution; b) frequency-domain solution

tained directly from the numerical integration scheme, while for the lattice-rod interface the contribution of the convolution integral is, although in an approximate sense, obtained analytically. Apparently, as a consequence, the numerical error for the discrete-continuous system is smaller and the obtained time-domain response is more precise.

Let us emphasize here that Fig. 3 and Fig. 4 are obtained for a dimensionless frequency $\Omega = 0,5$, for which, as shown by Fig. 2a, the dynamic stiffnesses of the cascade and the rod are similar. At higher frequencies, as the difference between the dynamic stiffnesses increases, it should be expected that, even for the time domain solution, the reflection at the lattice-rod interface will be larger than the reflection at the lattice-cascade interface.

Based on the above, it is legitimate to state that, for coupled systems, the governing system of equations of motion should preferably be solved in the frequency domain rather than in the time domain. Naturally, nonlinear phenomena cannot be described in the frequency domain and coupled systems that allow for nonlinear behaviour must generally be solved in the time domain. Nevertheless, as long as nonlinearities occur instantly and the system response can be considered piecewise linear, the response can be obtained by solving its system of equations algebraically in the frequency domain using the mixed time-frequency domain method proposed by Hoving and Metrikine [10].

REFERENCES

1 Radjai, F. and Dubois, F. Discrete-element Modeling of Granular Materials. Wiley-ISTE, (2011).

2 Fakhimi, A. A hybrid discrete–finite element model for numerical simulation of geomaterials, *Computers and Geotechnics*, **36**, 386-395, (2009).

3 Lisjak, A. and Grasselli, G. A review of discrete modeling techniques for fracturing processes in discontinuous rock masses, *Journal of Rock Mech. and Geotechnical Eng.*, **6**, 301-314, (2014).

4 Dorival, O., Metrikine, A. V. and Simone, A. A lattice model to simulate ice-structure interaction, *ASME 27th International Conf. on Offshore Mech. and Arctic Eng. (OMAE)*, (2008).

5 Dieterman, H. A. and Metrikine, A. V. Eigenfrequencies and simplified models of semi-infinite cascades with variable boundary mass, *Short communications on Math. Mech.*, **77** (3), 232-235, (1997).

6 Hoving, J. S. and Metrikine, A. V. On the coupling of nonlinear discrete element models with continua in the time domain, *XXXVIII Summer School Conf. on Adv. Problems in Mech.*, 22-27 June, (2010).

7 Maradudin, A. A., Montroll, E. M. and Weiss, G. H. Theory of Lattice Dynamics in the Harmonic Approximation. *Solid State Physics*. Academic Press, New York, (1963).

8 Metrikine, A. V., Kudarova, A. M., Hoving, J. S. and van Vliet, R. On the minimization of wave reflection at the interface of a discrete system and a dispersively-similar continuum., *Journal of Sound and Vibration*, **346**, 191-199, (2015).

9 Abramowitz, M. and Stegun, I. A. *Handbook of Mathematical Functions with Formulas, Graphs, and Mathematical Tables, 9th printing*, Dover, New York, (1972).

10 Hoving, J. S. and Metrikine, A. V. A mixed time-frequency domain method to describe the dynamic behaviour of a discrete medium bounded by a linear continuum, *XLIII Summer School Conf. on Adv. Problems in Mech.*, (2015).